Journal of Cerebral Blood Flow & Metabolism (2014) 34, 1472–1482

www.jcbfm.com

ORIGINAL ARTICLE

Ablation of *MMP9* gene ameliorates paracellular permeability and fibrinogen–amyloid beta complex formation during hyperhomocysteinemia

Nino Muradashvili, Reeta Tyagi, Naira Metreveli, Suresh C Tyagi[1] and David Lominadze[1]

Increased blood level of homocysteine (Hcy), called hyperhomocysteinemia (HHcy) accompanies many cognitive disorders including Alzheimer's disease. We hypothesized that HHcy-enhanced cerebrovascular permeability occurs via activation of matrix metalloproteinase-9 (MMP9) and leads to an increased formation of fibrinogen–β-amyloid (Fg–Aβ) complex. Cerebrovascular permeability changes were assessed in C57BL/6J (wild type, WT), cystathionine-β-synthase heterozygote (Cbs $+/-$, a genetic model of HHcy), *MMP9* gene knockout (Mmp9 $-/-$), and *Cbs* and *Mmp9* double knockout (Cbs $+/-$/Mmp9 $-/-$) mice using a dual-tracer probing method. Expression of vascular endothelial cadherin (VE-cadherin) and Fg–Aβ complex formation was assessed in mouse brain cryosections by immunohistochemistry. Short-term memory of mice was assessed with a novel object recognition test. The cerebrovascular permeability in Cbs $+/-$ mice was increased via mainly the paracellular transport pathway. VE-cadherin expression was the lowest and Fg–Aβ complex formation was the highest along with the diminished short-term memory in Cbs $+/-$ mice. These effects of HHcy were ameliorated in Cbs $+/-$/Mmp9 $-/-$ mice. Thus, HHcy causes activation of MMP9 increasing cerebrovascular permeability by downregulation of VE-cadherin resulting in an enhanced formation of Fg–Aβ complex that can be associated with loss of memory. These data may lead to the identification of new targets for therapeutic intervention that can modulate HHcy-induced cerebrovascular permeability and resultant pathologies.

Journal of Cerebral Blood Flow & Metabolism (2014) **34,** 1472–1482; doi:10.1038/jcbfm.2014.102; published online 28 May 2014

Keywords: caveolae; matrix metalloproteinase-9; memory loss; paracellular transport pathway; vascular endothelial cadherin

INTRODUCTION

Homocysteine (Hcy) is a highly reactive, sulfur-containing non-protein amino acid. It is synthesized from methionine by the removal of its terminal methyl group leading to the conversion of methionine to cysteine.[1] Hcy is metabolized by transsulfuration (depending on pyridoxine, vitamin B_6) and remethylation (depending on folic acid, vitamin B_9 and cobalamin, vitamin B_{12}) pathways.[2] In normal conditions, plasma content of Hcy varies from 3 to 15 μmol/L and higher plasma levels are considered as hyperhomocysteinemia (HHcy). There are three levels of HHcy: mild (15 to 30 μmol/L), moderate (30 to 100 μmol/L), and severe (>100 μmol/L).[3] Elevated blood level of Hcy is considered to be an independent and high-risk factor for many cardiovascular and cerebrovascular disorders such as atherosclerosis[4] and stroke.[5]

Many inflammatory disorders are accompanied by alterations in the blood–brain barrier (BBB) that result in leakage of plasma substances and proteins to interstitium[6] and may exacerbate complications of blood circulation during vascular diseases and cause edema.[6,7] Plasma proteins may cross the endothelial barrier through two main pathways: paracellular and transcellular.[6,8] Movement of substances via paracellular pathway occurs between the endothelial cells (ECs) and involves alterations in their junction proteins (JPs).[6] Transcellular transport is implemented by movement of substances across an EC and involves caveolae-mediated transcytosis.[9] Thus, the combination and the functional balance of these two pathways govern the net transport of substances between the blood stream and interstitium. Because caveolae-mediated transcytosis and paracellular transport are interconnected,[10] prevailing role of one or the other pathway in overall protein crossing of vascular wall is very difficult to define.

Presence of endothelial-specific adhesion molecule, vascular endothelial cadherin (VE-cadherin), which is exclusively expressed and located at the basal side of the EC contacts,[6,11] is an essential step that indicates the extent of permeability of blood vessels through the paracellular pathway.[11] Clathrin-, lipid raft-, or caveolae-mediated endocytosis is considered as means of transcellular transport.[12] In intestinal cells, endocytosis involves clathrin-coated pits that internalize cargo and deliver it to other cellular destinations. However, transendothelial transport in blood vessels does not conform to this scenario.[12] Caveolae, caveolae-generated transendothelial channels, and fenestrae are responsible for transcellular transport, i.e., transcytosis in ECs.[8] In contrast to the classic clathrin-dependent endocytosis, the caveolar transcytosis pathway avoids the lysosomes.[13] Thus, caveolae-mediated transcytosis is the primary transport mechanism by which plasma macromolecules traverse the endothelium.[14] Plasmalemmal vesicle-associated protein-1 (PV-1) is an integral membrane-associated protein of caveolae found in fenestral and stomatal diaphragms in the fenestrated endothelial and transendothelial channels.[15] It is considered a functional biomarker for

Department of Physiology and Biophysics, University of Louisville, School of Medicine, Louisville, Kentucky, USA. Correspondence: Dr D Lominadze, University of Louisville, Department of Physiology & Biophysics, School of Medicine, Building. A, Room 1115, 500 South Preston Street, Louisville, KY 40202, USA.
E-mail: david.lominadze@louisville.edu
Supported in part by NIH grants HL-071010, NS-051568, and NS-084823.
[1]These authors equally contributed to this work.
Received 2 December 2013; revised 22 April 2014; accepted 1 May 2014; published online 28 May 2014

caveolae along with Caveolin-1 (Cav-1), which is one of the main components of caveolae wall.[16]

We have already shown that high level of Hcy mediates macromolecular leakage in mouse brain pial microvessels and involves activation of matrix metalloproteinases.[17] Matrix metalloproteinases, zinc-dependent endoproteinases, are expressed in various cell types including ECs. Matrix metalloproteinases are involved in both physiologic and pathologic processes, especially in the subendothelial matrix (SEM) degradation and vascular remodeling that disrupt the BBB.[18] Activation of matrix metalloproteinase-9 (MMP9), the most abundant MMP, is involved in the decrease of brain vascular endothelial layer integrity through degradation of EC JPs and leads to macromolecular leakage.[18]

Besides being an inflammatory pathology, HHcy is associated with dementia and Alzheimer's diseases.[19] It is well known that microvascular deposition of the amyloid beta (Aβ) protein in brain is a prominent pathologic feature of Alzheimer's disease and is associated with dementia. It has been noted that deposition of the Aβ in the walls of cerebral vessels, known as cerebral amyloid angiopathy[20] triggers the degeneration of vessel wall components that can affect cerebral blood flow[21] and worsen cognitive decline.[22] Besides in the human brain, changes in levels of Aβ40 and Aβ42 have also been found in C57BL/6 mouse brain samples.[23] In addition, amyloid precursor protein accumulations were found in brains of injured C57BL/6 mice.[24] As another inflammatory agent, Fg is associated with an increased risk of Alzheimer's diseases.[25] It has been suggested that the interaction between Aβ and Fg may be an important contributor to Alzheimer's disease pathogenesis.[26] In the present study, we hypothesized that HHcy, via increasing cerebrovascular permeability, exacerbates Aβ binding to Fg and to collagen. Collagen is an important component of extracellular matrix, which can also be modified during HHcy.[27] It has been found that level of collagen is increased in cerebral microvessels during Alzheimer's disease.[28] Although the biologic function and the contribution of collagen to the pathogenesis of Alzheimer's disease and Aβ plaque formation are unknown, collagen binding to Aβ has been documented.[25] Thus, collagen can be a base matrix for Fg and Aβ deposition in SEM and possible formation of Aβ-Fg-collagen complex may be associated with cognitive dysfunction.

The purpose of the present study is to define: (1) the prevailing role of paracellular or transcellular pathway in HHcy-induced cerebrovascular leakage, (2) the extent of Aβ–Fg–collagen complex formation during HHcy, (3) possible changes in cognitive function, particularly in short-term memory using a novel object recognition test in HHcy mice, and (4) the role of *MMP9* gene ablation in Aβ–Fg–collagen complex formation.

MATERIALS AND METHODS

Animals

In accordance with the National Institute of Health Guidelines for animal research, all animal procedures for these experiments were reviewed and approved by the Institutional Animal Care and Use Committee of the University of Louisville.

Male wild-type (WT) C57BL/6J, *MMP9* gene knockout (Mmp9 $-/-$) homozygous (FVB.Cg-*Mmp9*^{tm1Tvu}/J; Stock Number: 004104) and cystathionine β-synthase (Cbs $+/-$) heterozygous (genetic model of mouse HHcy, Stock Number: B6129P2) mice were obtained from the Jackson Laboratory (Bar Harbor, ME, USA).

Cbs $+/-$/Mmp9 $-/-$ double knockout animals were obtained by crossbreeding of Cbs $+/-$ and Mmp9 $-/-$ mice. For genotyping of Cbs $+/-$/Mmp9 $-/-$ mice, DNA was extracted from the tail tip of the mice and was amplified by polymerase chain reaction using specific primer sequences according to the protocol provided by the Jackson Laboratory and presented previously.[29] The primer sequences to identify Mmp9 $-/-$ were forward: 5- CTG AAT GAA CTG CAG GAC GA-3′; reverse: 5′-ATA CTT TCT CGG CAG GAG CA 3′ for MMP9 mutations and for WT were forward: 5′-GTG GGA CCA TCA TAA CAT CAC A-3′; reverse: 5′-CTC GCG GCA AGT CTT CAG AGT A-3′. The primer sequences to identify *Cbs* gene mutation were as follows: reverse 5′-CGT GCA ATC CAT CTT GTT CA-3′ for *Cbs* mutant, reverse 5′-AGC CAA CTT AGC CCT TAC CC-3′ for WT, and forward 5′-GAT TGC TTG CCT CCC TAC TG-3′ for common.

Reagents and Antibodies

Fluorescein isothiocyanate (FITC) was from Sigma-Aldrich Chemicals (St Louis, MO, USA). Alexa Fluor 647-conjugated bovine serum albumin (BSA-Alexa Fluor-647) and secondary antibodies conjugated with Alexa-fluor 488, Alexa Fluor 594, or Alexa Fluor 647 were purchased from Invitrogen (Carlsbad, CA, USA). Goat polyclonal anti-mouse VE-cadherin (Cdh5, clone: C-19), Goat polyclonal anti-collagen antibody COL4A1/5 (C-19, epitope near the C-terminus of Collagen α-type IV, detects Collagen α1 and α5 type IV in mouse) and 4′,6-diamidino-2-phenyl-indole HCl were from Santa Cruz Biotechnology (Santa Cruz, CA, USA). Rabbit polyclonal antibody against Cav-1 was obtained from Novus Biological (Littleton, CO, USA). Rat anti-mouse PV-1 monoclonal antibody (clone: MECA-32; Isotype: IgG2a) was from AbD Serotec (Raleigh, NC, USA). Human EC lysate was purchased from BD Biosciences (San Diego, CA, USA). Polyclonal rabbit anti-human Fg antibody (detects native Fg as well as Fg fragments D and E) was from Dako (Carpinteria, CA, USA). Rabbit polyclonal anti-Aβ antibody (ab2539), which identifies amino-acid residues 1–14 of Aβ and stains extracellular aggregates of Aβ peptides, was obtained from Abcam (Cambridge, MA, USA). Radio-Immunoprecipitation Assay buffer was from Boston BioProducts (Worcester, MA, USA) while normal donkey serum was obtained from Jackson ImmunoResearch (West Grove, PA, USA). Tetramethylrhodamine β-isothiocyanate- or FITC-conjugated *Lycopersicon esculentum* agglutinin (LEA) tomato lectin was from Vector Laboratories (Burlingame, CA, USA). Artificial cerebrospinal fluid was purchased from Harvard Apparatus (Holliston, MA, USA).

Cranial Window Preparation

Fourteen-week old mice (body weight ranged from 28 to 32 g) were anesthetized with sodium pentobarbital (70 mg/kg, intraperitoneal). Brain pial microcirculation was prepared for observations as previously described.[17,29–31] Briefly, a mouse was placed on a stereotaxic apparatus (World Precision Instruments, Sarasota, FL, USA). The scalp and connective tissues were removed over the parietal cranial bone above the left hemisphere. A craniotomy ($\sim$4 mm in diameter) was done with a high-speed microdrill (Fine Science Tools, Foster City, CA, USA). The dura matter was lifted with the bone disk using an extra-fine tip micro-rongeur (Fine Science Tools). The surface of the exposed pial circulation was continuously superfused with cerebrospinal fluid. Constant temperature (37 °C) of cerebrospinal fluid was maintained by dual automatic temperature controller (Warner Instrument Corporation, Hamden, CT, USA).

Microvascular Leakage Observation

A dual-tracer probing method[30] was used to define a prevailing role of transcellular versus paracellular transport mechanisms induced by HHcy. Briefly, after the surgical preparation, there was a 1-hour equilibration period. Before each experiment, autofluorescence of the observed area was recorded over a standard range of camera gains. Mixture of 100 μL of FITC (300 μg/mL) and 20 μL of BSA-Alexa Fluor-647 (3.3 mg/mL) in phosphate-buffered saline was infused through the cannulated carotid artery. The solution was infused with a syringe pump (Harvard Apparatus) at 30 μL/min speed and allowed to circulate for 10 minutes.[17,29] The pial circulation was surveyed to ensure that there was no spontaneous leakage of BSA-Alexa Fluor-647 in the observed area that would indicate compromised vascular integrity. Venules were identified by the topology of the pial circulation and blood flow direction. Images of the selected third-order venular segments were recorded and used as baseline. After obtaining the baseline reading, images of the venular segments were recorded at 10, 20, 40, 60, and 90 minutes.

An epi-illumination system was used to observe intravascular and extravascular FITC and BSA-Alexa Fluor-647. The area of interest was exposed to blue light (488 nm) and then red light (647 nm) for 10 to 15 seconds with a power density of 3.5 μW/cm^2. The microscope images were acquired by an electron-multiplying charge-coupled device camera (Quantem 512SC, Photometrics, Tucson, AZ, USA) and image acquisition system (Slidebook 5.0, Intelligent Imaging Innovations, Philadelphia, PA, USA). The camera output was standardized with a 50 ng/mL fluorescein diacetate standard (Estman Kodak, Rochester, NY, USA) for each experiment. The lamp power and camera gain settings were held constant

during experiments, and the camera response was verified to be linear over the range used for these acquisitions. The magnification of the system with Olympus × 20/0.40 (UPlanSApo) objective was determined with a stage micrometer.

Images of the pial venular circulation were analyzed by image analysis software (Imagepro Plus 7.0, Media Cybernetics, Bethesda, MD, USA). In each image, a 30 μm in length line profile probe was positioned in the middle of the vessel and outside of a venular wall in parallel to the venule. Mean fluorescence intensities along the line profile probes were measured for each dye and leakage of FITC or BSA-Alexa Fluor-647 to interstitium was assessed by changes in the ratio of fluorescence intensity of each dye in the interstitium to that inside the venule for the respective dye. The results were averaged for each experimental group and presented as percent of baseline.

Collection of Brain Samples

At the completion of experiments, animals were exsanguinated to collect brain samples for western blot analyses. To assess content of Cav-1 and PV-1, brain samples were digested in Radio-Immunoprecipitation Assay buffer (20 g of tissue/1 mL of Radio-Immunoprecipitation Assay buffer) in the presence of protease inhibitor cocktail (Sigma). The samples were homogenized using Ten Broek Tissue Grinder (Corning Incorporated, Corning, NY, USA) at 4°C. After homogenization, samples were centrifuged at 16,000 g for 10 minutes. The supernatant was centrifuged again at 16,000 g for 10 minutes to separate leftover tissue debris. The supernatant was collected and total protein content was determined by Bradford method.

For immunohistochemistry, in the separate series of experiments, mice were infused with FITC- or tetramethylrhodamine β-isothiocyanate-conjugated LEA via the carotid cannulation to fluorescently label moieties on the intravascular surface.[29] Animals killed with an anesthetic overdose were immediately infused with phosphate-buffered saline through the left ventricle for exsanguination. After the cranium was opened, the brain was gently dissected and removed for fresh tissue processing. Brain samples mounted in protective matrix (Polyscience, Warrington, PA, USA) were cryosectioned with a Leica CM 1850 Cryocut (Bannockburn, IL, USA) into 15-μm thick slices and stored at −80 °C.

Immunohistochemistry

Mouse brain tissue immunohistochemical analysis was done according to the method described earlier.[29] Briefly, after warming the slides at 37 °C for 20 minutes and removing the mounting matrix, the sections were postfixed in ice-cold 100% methanol for 10 minutes, washed three times in Tris-buffered saline and blocked for non-specific epitope binding in 0.1% Triton X-100 Tris-buffered saline, 0.5% BSA, and 10% normal donkey serum for 1 hour at room temperature.

Primary antibodies such as anti-VE-cadherin (dilution 1:250), anti-Cav-1 (dilution 1:100), anti-PV-1 (dilution 1:100), anti-Aβ (dilution 1:150), anti-Collagen (dilution 1:150), or anti-Fg (dilution 1:200) were applied to the brain slices. After washing, appropriate fluorescent dye-conjugated secondary antibodies (dilution 1:500) were applied to the brain slices for 1 hour at room temperature. Cell nuclei were labeled with 4′,6-diamidino-2-phenyl-indole HCl (1:1,000). The laser-scanning confocal microscope (Olympus Fluo-View1000, with objective × 60) was used to capture images. VE-cadherin and tetramethylrhodamine β-isothiocyanate-LEA were visualized using a HeNe-Green laser (543 nm) to excite the dye, while emission was observed above 573 nm. FITC-LEA or Aβ were visualized using a multiline argon-ion laser (458/488/515 nm) to excite the dye, while emission was observed above 519 nm. Fg and collagen were visualized using a HeNe-Red laser (633 nm). Cell nuclei were visualized using a blue Laser Diode (405 nm) to excite the dye (4′,6-diamidino-2-phenyl-indole HCl), while emission was observed above 456 nm. Fluorescence intensity (for each color) was adjusted to its saturation point in an experimental group with the maximum fluorescence intensity for the color of interest and the laser and multipliers' settings were kept unaltered during measurements in each experimental series. Before assessing expressions or co-localizations of proteins of interest by confocal microscopy, levels of autofluorescence, determined by each specific primary antibody used in the study, were measured in control samples. Results showed that autofluorescence of samples were neglectable. Therefore, although included in image analysis, autofluorescence values of samples are not reported. In addition, levels of fluorescence generated by secondary antibodies alone were measured and found almost nonexistent.

Off-line image analysis software (Imagepro Plus) was used to assess expression of VE-cadherin, PV-1, Cav-1, and deposition of Fg and Aβ on vascular matrix collagen in brain samples. Fluorescence intensity was measured in the area of interest placed along the vessel wall and normalized per length of the respective vascular segment. For each experimental group, 4 to 5 brain slices were analyzed. In each brain slice, three to five vessels were analyzed. Fluorescence intensity in eight randomly placed constant size area of interests were measured. The results were averaged for each experimental group and values were presented as fluorescence intensity units (FIU). Co-localizations of Cav-1 and PV-1, Fg and Aβ, and Aβ and collagen in brain vessels were assessed by measuring number of spots generated after co-localization of respective colors in images formed after deconvolution of original images as described earlier.[32] Resolution of presented images is 2.84 pixel/mm (width-279 pixels, height-259 pixels).

Western Blot Analysis

Equal volume (30 μL) of protein from each animal group were loaded onto 8% SDS–PAGE gels and electrophoresed under reducing conditions and then transferred onto nitrocellulose membranes. Cell lysate was used as positive control to detect Cav-1 band. After blocking of membranes with 5% non-fat dry milk in TBS-T, membranes with brain samples were incubated with anti-Cav-1 or anti-PV-1 antibodies overnight at 4 °C. Then, probing with appropriate secondary antibodies for 2 hours at room temperature, the blots were developed using a Bio-Rad Molecular Imager (ChemiDoc XRS+, Hercules, CA, USA). The blots were analyzed with ImagePro Plus. The levels of protein expressions were assessed by measuring an integrated optical density (IOD) of bands of interest and GAPDH bands in the lane profile. Results were presented as ratio of the IOD of each band of interest to the IOD of the respective GAPDH band.

Novel Object Recognition Test

The novel object recognition test was performed using a Top Scan behavioral analyzing system (Version 3.00 by CleverSys; Reston, VA, USA). Short-term memory of mice was assessed according to the method described elsewhere.[33] Briefly, after 2 days of acclimatization after transportation, the animals were trained during 3 days for 10 minutes twice a day. On the day of experiment, two similar objects were placed in the box. The animal was placed at the mid-point of the wall opposite to objects for 5 minutes. After an hour, one of the objects was replaced with a novel object and the animal was returned to the box for 3 minutes. The behavioral assessment was provided by calculating discrimination ratio (DR, time spent at the novel object/time spent at both objects). Low DR (lesser interest and time spent to the novel object) indicates an impairment of memory.[33]

Data Analysis

All data are expressed as mean ± s.e.m. The experimental groups were compared by one-way analysis of variance. Differences in cerebrovascular permeability to two tracers were analyzed with repeated measures analysis of variance. If analysis of variance indicated a significant difference ($P<0.05$), Tukey's multiple comparison test was used to compare group means. Differences were considered significant if $P<0.05$.

RESULTS

Animal Genotyping

Genotyping of experimental animals using appropriate primers and polymerase chain reaction positively indicated that in comparison with WT mice, Cbs+/− and Mmp9−/− mice lack *Cbs*[34] and *MMP9*[29] genes, respectively. Genotyping of new Cbs+/−/Mmp9−/− mice showed that they lack both *Cbs* and *MMP9* genes (Figure 1, Inset).

Macromolecular Leakage from Pial Venules

To define prevailing role of paracellular or transcellular transport in overall cerebrovascular permeability at elevated level of Hcy, pial venular permeabilities to two, high- and low-molecular weight (MW) tracers were compared.[30] We found that pial venular permeability was increased during HHcy affecting both transcellular and paracellular pathways (Figure 1). Data showed that venular leakage to FITC, a low MW tracer used as a marker of paracellular transport,[30] increased steadily after 30 minutes from the beginning of observation (Figure 1B). It was accompanied with

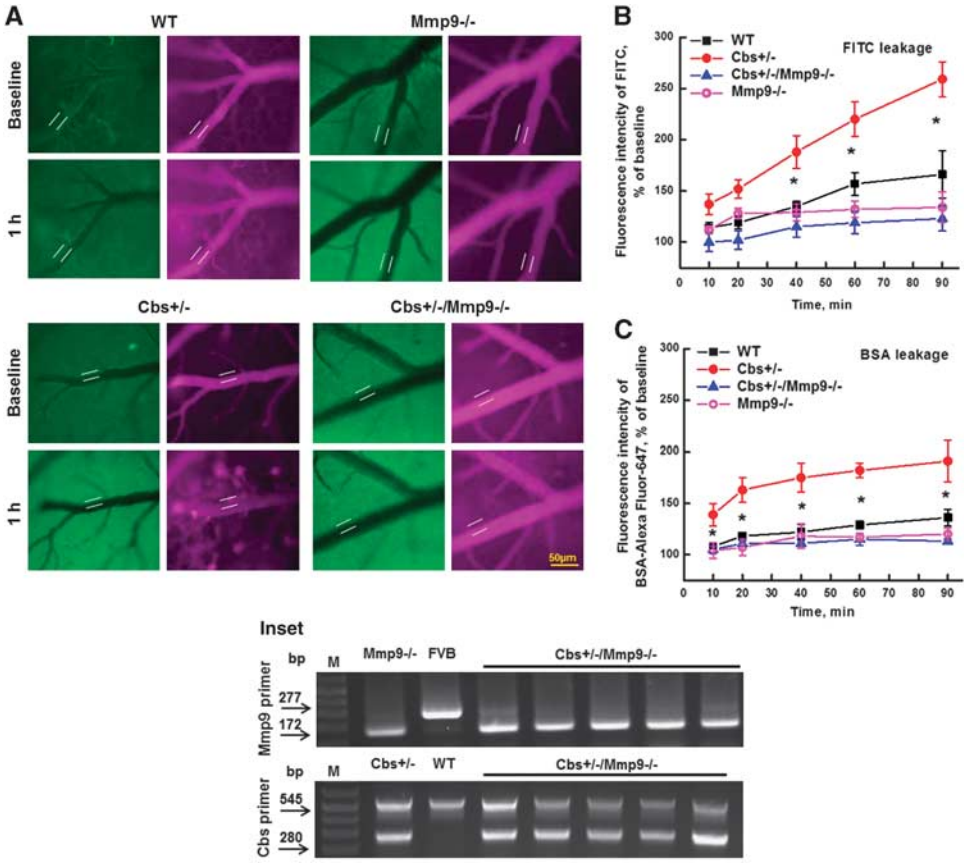

Figure 1. Hyperhomocysteinemia (HHcy)-induced leakage of mouse pial venules. A dual-tracer probing method was used to define prevailing role of paracellular versus transcellular transport in pial venules of WT, *Cbs* gene knockout heterozygous (Cbs + / −), *MMP9* gene knockout (Mmp9 − / −), and Cbs + / − and Mmp9 − / − double knockout (Cbs + / − /Mmp9 − / −) mice. (**A**) Examples of images recorded immediately (baseline) and after 1 hour after infusion of fluorescein isothiocyanate (FITC) (green) and Alexa-647- conjugated bovine serum albumin (BSA) (red) tracers. Microvascular permeability was assessed by comparison of ratios of fluorescence intensities of dyes measured along the line profile probe (LPP) outside to that of inside of the vessel shown on images. Summary of changes in LLP ratios of fluorescence intensity values of FITC (**B**) and BSA-Alexa Fluor-647 (**C**) tracers. *$P < 0.05$, versus WT; $n = 8$ for all groups. Inset: Genotyping of *Cbs* and *Mmp9* gene double knockout (Cbs + / − /Mmp9 − / −) mice. Dual polymerase chain reaction (PCR) products suggest the heterozygous mutation of *Cbs* gene (Cbs + / −) and single PCR product suggests homozygous mutation of *Mmp9* gene (*Mmp9* − / −) while their absence represents FVB or wild-type (C57BL) alleles.

accumulation of BSA-Alexa Fluor-647, a high-MW tracer,[30] in the interstitium starting from the 10th minute of observation (Figure 1C). These effects were ameliorated in Cbs + / − / Mmp9 − / − mice (Figure 1). Pail venular permeability to FITC or to BSA-Alexa Fluor-647 in Mmp9 − / − mice was not different from that in WT mice, respectively (Figure 1).

VE-Cadherin Expression in Mouse Brain Vessels

Expression of VE-cadherin (red) in brain cortical vessels was lesser in Cbs + / − mice (8.4 ± 0.7 FIU) than in WT (16.4 ± 1.8 FIU) or Mmp9 − / − (16.3 ± 4.7 FIU) mice (Figure 2). In Cbs + / − / Mmp9 − / − mice VE-cadherin expression (11.1 ± 0.4 FIU) was greater than in Cbs + / − mice (Figure 2). However, it was still lesser than in vessels of WT mice (Figure 2). The endothelial marker, LEA is shown in green color and cell nuclei labeled with 4′,6-diamidino-2-phenyl-indole HCl are in blue (Figure 2A).

Cav-1 and PV-1expression and their co-Localization in Mouse Brain Vessels

There was no difference in expression of Cav-1 (red) in Cbs + / − mice (47.3 ± 3.4 FIU) compared with that in WT (40.2 ± 2.5 FIU), Mmp9 − / − (40.1 ± 3.7 FIU), or Cbs + / − /Mmp9 − / − (46 ± 4.1 FIU) animals (Figures 3A and 3B). Expression of PV-1 (green) in Cbs + / − mice (44.9 ± 2.8 FIU) was not statistically different from that in WT (45.4 ± 1.7 FIU) but was significantly less compared with that in Mmp9 − / − (57.8 ± 4.5 FIU) and Cbs + / − /Mmp9 − / − (52.6 ± 3.4 FIU) mice (Figures 3A and 3C). Caveolae (yellow) formation (defined by spots with co-localized Cav-1 and PV-1) was similar in all animal (WT (211 ± 12), Cbs + / − (233 ± 15), Cbs + / − /Mmp9 − / − (225 ± 12) and Mmp9 − / − (245 ± 10) groups (Figures 3A and 3D). The endothelial marker, LEA is shown in blue color (Figure 3A).

Cav-1 and PV-1 Expression in Mouse Brain Samples

Expression of Cav-1 (Figures 3E and 3F) in brains from Cbs + / − mice (0.33 ± 0.02 IOD) was not different from that in WT (0.3 ± 0.02 IOD), Mmp9 − / − (0.31 ± 0.04 IOD), or Cbs + / − /Mmp9 − / − (0.38 ± 0.04 IOD) animals (Figures 3E and 3F). Expression of PV-1 (Figures 3G and 3H) was less in Mmp9 − / − (0.38 ± 0.04 IOD) and Cbs + / − /Mmp9 − / − (0.36 ± 0.01 IOD) mice compared with that in WT (0.6 ± 0.04 IOD) or Cbs + / − (0.57 ± 0.02 IOD) mice (Figures 3G and 3H).

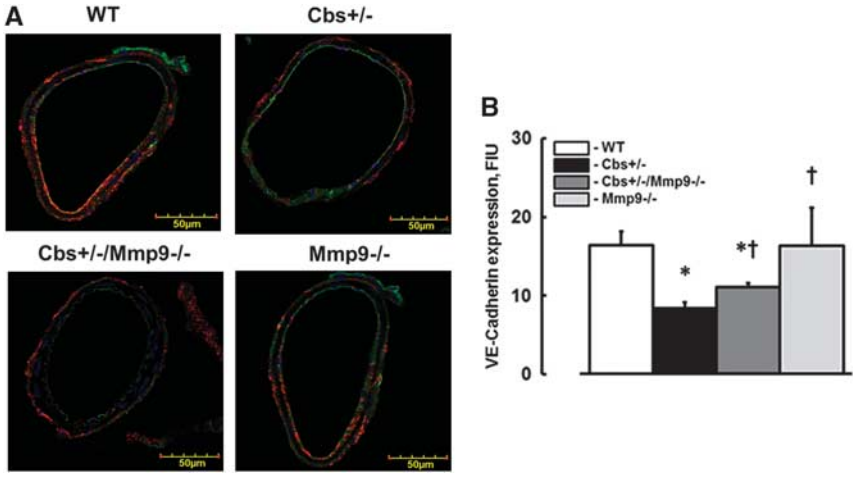

Figure 2. Expression of vascular endothelial cadherin (VE-cadherin) in mouse brain vessels. (**A**) Examples of vessel images in samples obtained from wild type (WT), Cbs $+/-$, Cbs $+/-$, and Mmp9 $-/-$ double knockout (Cbs $+/-$/Mmp9 $-/-$), and *MMP9* gene knockout (Mmp9 $-/-$) mice. VE-cadherin expression was assessed by fluorescence intensity along the vascular segment. Expression of VE-cadherin (red) in cortical vessels shown with FITC-LEA-labeled endothelium (green) and 4′,6-diamidino-2-phenyl-indole HCl-labeled nuclei (blue). (**B**) Summary of VE-cadherin fluorescence intensity changes in vascular segments. *$P<0.05$ for all, versus WT; †, versus Cbs $+/-$; $n=5$ for all groups.

Aβ and Fg Deposition and their Co-Localization in Mouse Brain Vessels

Depositions of Aβ (green) and Fg (red) were greater (5.0 ± 0.7 and 19.0 ± 1.2 FIU, respectively) in cortexes of Cbs $+/-$ mice compared with those (2.1 ± 0.4 and 15.0 ± 1.1 FIU, respectively) in WT, (2.0 ± 0.1 and 14.0 ± 1.1 FIU, respectively) Mmp9 $-/-$, or (1.0 ± 0.1 and 13.0 ± 1.1 FIU, respectively) in Cbs $+/-$/Mmp9 $-/-$ animals (Figures 4A–C). Co-localization (yellow, indicated by arrows) of Aβ and Fg in vascular segments of these brain samples indicated formation of Fg–Aβ complexes (Figures 4A and 4D). The number of co-localized spots were more in brain samples from Cbs $+/-$ mice (76 ± 28) compared with that in samples from WT (25 ± 4) and Mmp9 $-/-$ (26 ± 8) mice (Figure 4D). Ablation of *MMP9* gene in HHcy mice ameliorated the formation of this complex (12 ± 8, the number of co-localized spots, Figure 4D). The endothelial marker, LEA is shown in blue color (Figure 4A).

Aβ and Collagen Deposition and their Co-Localization in Mouse Brain Vessels

Deposition of Aβ (green) and formation of collagen (red) were more in Cbs $+/-$ mice (79 ± 5.7 and 64.4 ± 8.5 FIU, respectively) compared with those in WT (6.9 ± 0.5 and 22.8 ± 1.5 FIU, respectively), Mmp9 $-/-$ (10.7 ± 1.3 and 17.4 ± 1.2 FIU, respectively), or Cbs $+/-$/Mmp9 $-/-$ (30.8 ± 4 and 33.7 ± 4 FIU, respectively) animals (Figures 5A–C). Deposition of Aβ on cerebrovascular collagen and Aβ-collagen (yellow, indicated by arrowheads) complex formation (defined by spots of co-localized Aβ and collagen) was greater in Cbs $+/-$ mice (27 ± 3 spots) compared with that in WT (7 ± 2 spots), Mmp9 $-/-$ (6 ± 3 spots), or in Cbs $+/-$/Mmp9 $-/-$ (8 ± 2 spots) mice (Figures 5A and 5D). The endothelial marker, LEA is shown in blue (Figure 5A).

Novel Object Recognition Test

Loss of short-term memory was greater in Cbs $+/-$ mice (DR $\sim 0.43\pm0.15$) compared with that in WT (DR $\sim 0.86\pm0.08$), Mmp9 $-/-$ (DR $\sim 0.88\pm0.07$) or Cbs $+/-$/Mmp9 $-/-$ (DR $\sim 0.63\pm0.17$) mice (Figure 6).

DISCUSSION

Although Fg and Aβ peptide plaque formation is the hallmark of Alzheimer's disease,[26] mechanisms of this plaque formation and its deposition in cerebral vasculature or SEM are not clear. Hyperhomocysteinemia has been identified as an independent risk factor for vascular dementia and stroke primarily causing an endothelial dysfunction.[35] In addition, it has been shown that an increased plasma Hcy level is associated with development of Alzheimer's disease.[19] Strong interaction between Hcy and Fg has been reported.[36] Elevated level of Hcy leads to Fg modifications that increase its resistance to fibrinolysis and thus make Fg deposits much stronger.[36] Thus, the first step in fibrinolysis resistant Fg–Aβ complex formation is to have conditions when Fg is immobilized, which allows its binding to Aβ. These conditions will most likely arise when Fg is bound to the vascular wall or as a result of this binding crosses the vessel wall and deposits in SEM. Thus, appearance of Fg–Aβ complex in SEM or extracellular tissue can be a result of changes in vascular permeability leading to leakage of Fg. This enhanced Fg deposition promotes binding of Fg to Aβ and thus, formation of Fg–Aβ complex. Presence of high level of Hcy can further increase the complex's resistance to fibrinolysis.[36]

We previously found that elevated level of Hcy decreased EC layer integrity (defined by changes in transendothelial electrical resistance) suggesting the wider opening of gaps between the ECs.[37] The present data confirmed the results of our other study where we showed that HHcy increased overall pial venular protein leakage but were unable to differentiate paracellular from transcellular transport.[17] Changes in EC layer integrity, the first level of BBB, define the permeability of cerebral vasculature. One of the tracers we used was FITC, a small MW molecule that can readily move through cell junctions as, for example, Lucifer Yellow, which is a known marker of paracellular transport.[38] Fluorescein isothiocyanate was used in conjunction with high-MW molecule, BSA, which can pass between the cells only if the cell junction gaps are opened wide enough, while it can cross endothelial layer via caveolar transcytosis when caveolae are functional. Our data indicate that pial venular leakage of FITC was greater in Cbs $+/-$ mice starting from 40th minute of observation compared with that in control mice. Similarly, BSA crossing of vascular wall was greater at each time point in these mice compared with those in control group. These effects are different from the effect of elevated level of Fg, called hyperfibrinogenemia (HFg), where HFg-induced cerebrovascular leakage of FITC via paracellular transport was only transiently greater than in control group, while

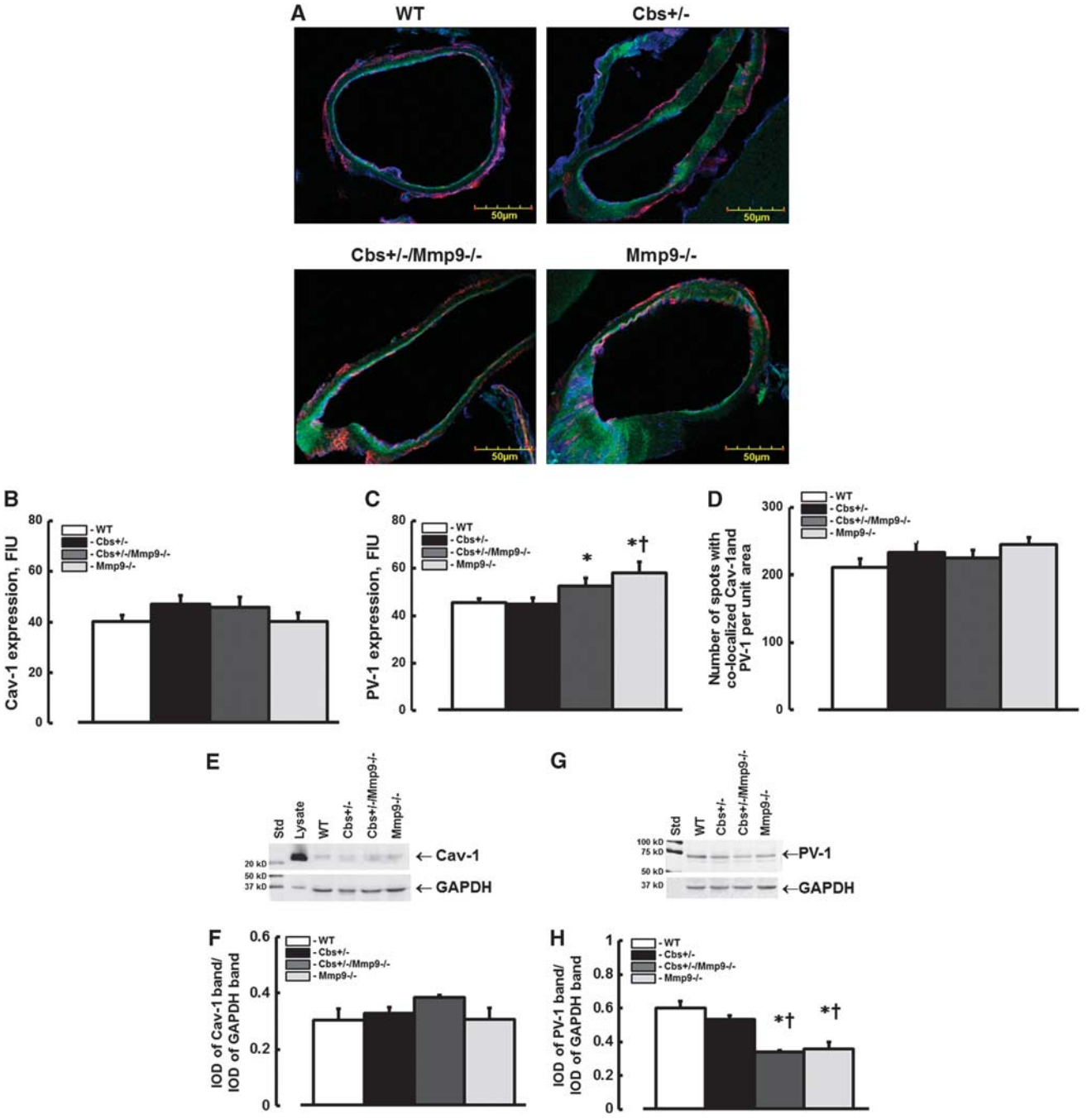

Figure 3. Expression caveolin-1 (Cav-1) and plasmalemmal vesicle-associated protein-1 (PV-1) in mouse brain vessels. (**A**) Examples of vessel images in samples obtained from wild type (WT), Cbs + / −, Cbs + / −, and matrix metalloproteinase-9 (Mmp9 − / −) double knockout (Cbs + / − /Mmp9 − / −), and *MMP9* gene knockout (Mmp9 − / −) mice; Expression of PV-1 (green) and Cav-1 (red) in cortical vessels shown with *Lycopersicon esculentum* agglutinin (LEA)-labeled endothelium (blue). (**B**–**D**) Summary of fluorescence intensity changes in brain cortical vessels defined by immunohistochemistry. Examples of western blot images of Cav-1 (**E**) and PV-1 (**G**) expressions in mouse brain cortical samples. Summary of ratios of integrated optical density (IOD) of Cav-1 (**F**) and PV-1 (**H**) bands from each group to those of the respective glyceraldehyde-3-phosphate dehydrogenase (GAPDH) bands. Note: Cell lysate (lysate) was used as a positive control for Cav-1. $^{*}P < 0.05$, versus WT; †, versus Cbs + / −; $n = 4$ for all groups.

BSA crossing of pial venular wall was greater at each time point than in control mice suggesting a prevailing role of transcellular transport pathway.[30] Combined, these results indicate that contrary to the effect of HFg, which affects mainly the transcellular transport,[30] HHcy affects mainly the paracellular rout.

Earlier we have shown that an elevated blood level of Hcy causes cerebrovascular protein leakage in mice and an increase in the formation of filamentous actin in cultured ECs.[17] Later we demonstrated that HHcy downregulates adherence junction protein, VE-cadherin and tight junction-associated protein, zonula occludin-1 (ZO-1) in cultured cells.[37] In the recent study, we found that injection of Hcy decreased messenger RNA of tight junction protein, occludin, and ZO-1 in mouse brain samples.[39] It is known that all these JPs are linked to cellular actin stress fibers.[6]

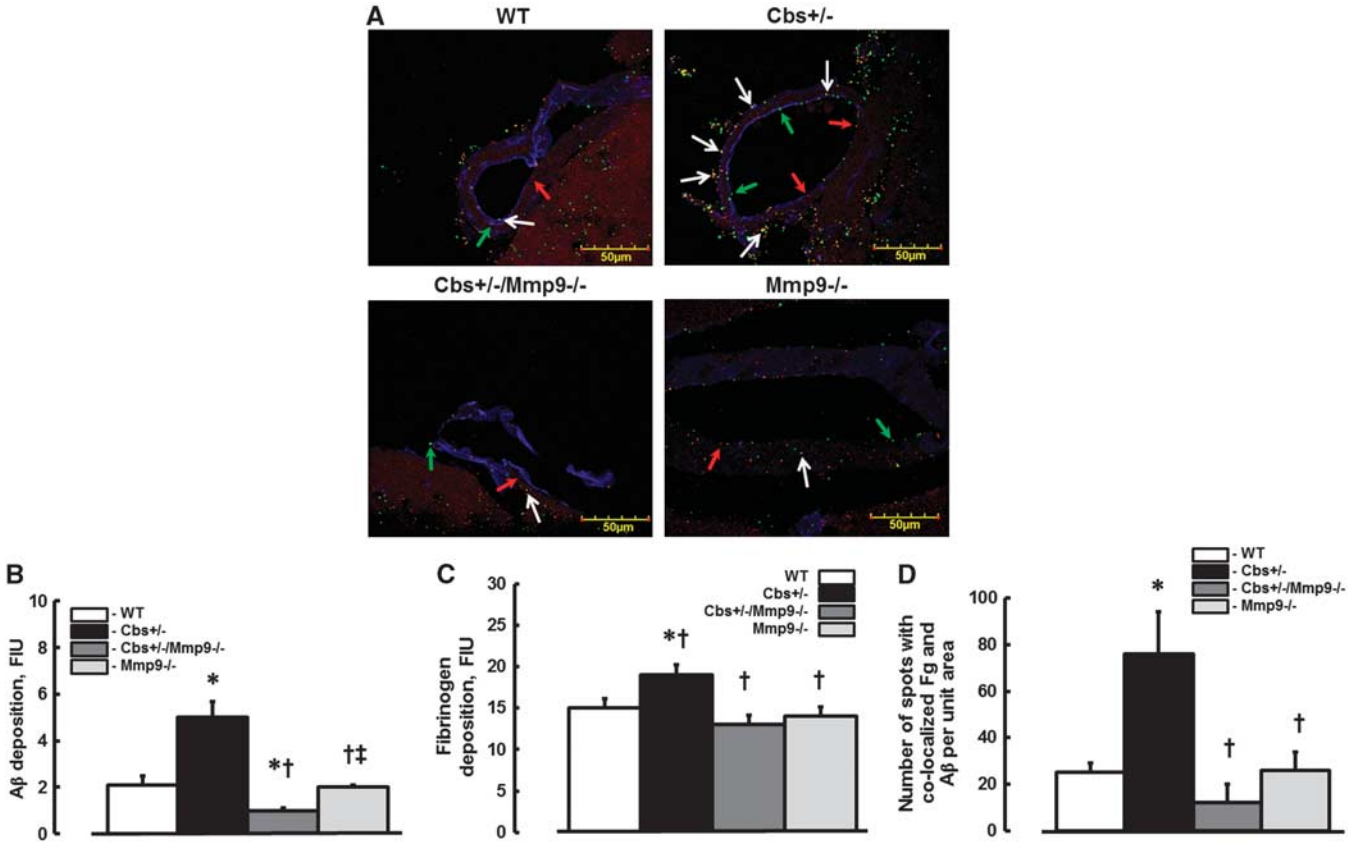

Figure 4. Deposition of fibrinogen (Fg) and amyloid beta (Aβ) in mouse brain vessels. (**A**) Examples of vessel images in samples obtained from wild type (WT), Cbs $+/-$, Cbs $+/-$, and matrix metalloproteinase-9 (Mmp9 $-/-$) double knockout (Cbs $+/-$/Mmp9 $-/-$), and *MMP9* gene knockout (Mmp9 $-/-$) mice. Deposition of Fg (shown as red dots and indicated with red arrows) and Aβ (shown as green dots and indicated with green arrows), and their co-localization (shown in yellow and indicated with white arrows) in brain vessels was assessed by measuring fluorescence intensities of Fg (red) and Aβ (green) and number of spots with co-localized green and red colors after deconvolution of images. Summaries of Aβ (**B**) and Fg (**C**) depositions and Fg and Aβ co-localization (**D**) assessments. *$P<0.05$ for all, versus WT; †, versus Cbs $+/-$; ‡, versus Cbs $+/-$/Mmp9 $-/-$; $n=5$ for all groups.

Therefore, HHcy-induced formation of filamentous actin would positively contribute to translocation of all JPs to cytosol and to the resultant opening of the gaps between the ECs. While tight and gap JPs primarily determine cell to cell interaction, VE-cadherin is the major determinant of EC contact integrity and cell to SEM interaction. Therefore, it has a prevailing role in the changes of blood vessel wall permeability for cells and large substances[40] such as high-MW proteins (e.g., albumin or Fg).

Previously, we found that high-Hcy diet increased blood pressure in normal C57BL/6J mice but did not affect blood pressure in Mmp9 $-/-$ mice.[41] We showed that HHcy-induced vascular remodeling inducing the arterial wall thickening may contribute to a decrease in arterial elasticity. In addition, effect of HHcy on vascular connexin-40 (connexin-40 has a crucial role in maintaining vasomotor tone) and decrease in elastin and endothelial nitric oxide synthase activity can be involved in vascular remodeling leading to elevated blood pressure. These effects were absent in Mmp9 $-/-$ mice. However, HHcy-induced activation of MMP9 in cultured ECs,[42] and HHcy-induced increased permeability of cultured ECs were ameliorated in the presence of MMP9 activity inhibitor.[41] These data suggest that HHcy directly activates MMP9 and absence of MMP9 activity prevents vascular remodeling, which leads to an increase in blood pressure and vascular permeability.

Our other studies indicate that HFg, although still alters JPs, mainly affects caveolar transcytosis.[30] In the present study, we found that HHcy most likely does not affect caveolar transcytosis. However, it enhances paracellular transport affecting JPs such as occludin, ZO-1,[37,39] and VE-cadherin via activation of MMP9 as seen in the present study. HHcy-mediated activated MMP9 can be involved in digestion of JPs between the ECs indicated by their translocation to the cellular cytosol.[37] This dual effect of HHcy most likely results in robust opening of gaps in EC layer and allows accumulation of large proteins such as Fg in SEM. These results coincide with data showing that an increased activity of MMP9 was associated with downregulation of tight-JPs such as ZO-1, occludin, and claudin-5 in brain microvessels of apolipoprotein E knockout apolipoprotein E $-/-$ mice.[43] In general, a strong association of increased permeability of brain capillaries with changes in expression of JPs (ZO-1, occludin, claudin-5, or VE-cadherin) has been demonstrated previously.[43,44]

As fibrin is a product of Fg, it is noteworthy to mention that accumulation of fibrin in perivascular area was particularly greater in brain capillaries lacking pericytes.[44] It is known that pericytes are involved in modulation of brain capillary diameter and their integrity.[44] Enhanced accumulation of Fg leads to favorable conditions for Fg–Aβ complex formation. It has been shown that clots formed from homocysteinylated Fg are more resistant to lysis than clots formed from native Fg.[36,45] Therefore, activation of MMP9 has lesser effect on Fg clots or Fg–Aβ complexes during HHcy than during normal level of Hcy. In addition, Hcy potentiates Aβ-induced neurodegeneration affecting cytosolic calcium.[46] Thus, formation of Fg–Aβ complex during HHcy has deleterious effect in brain.

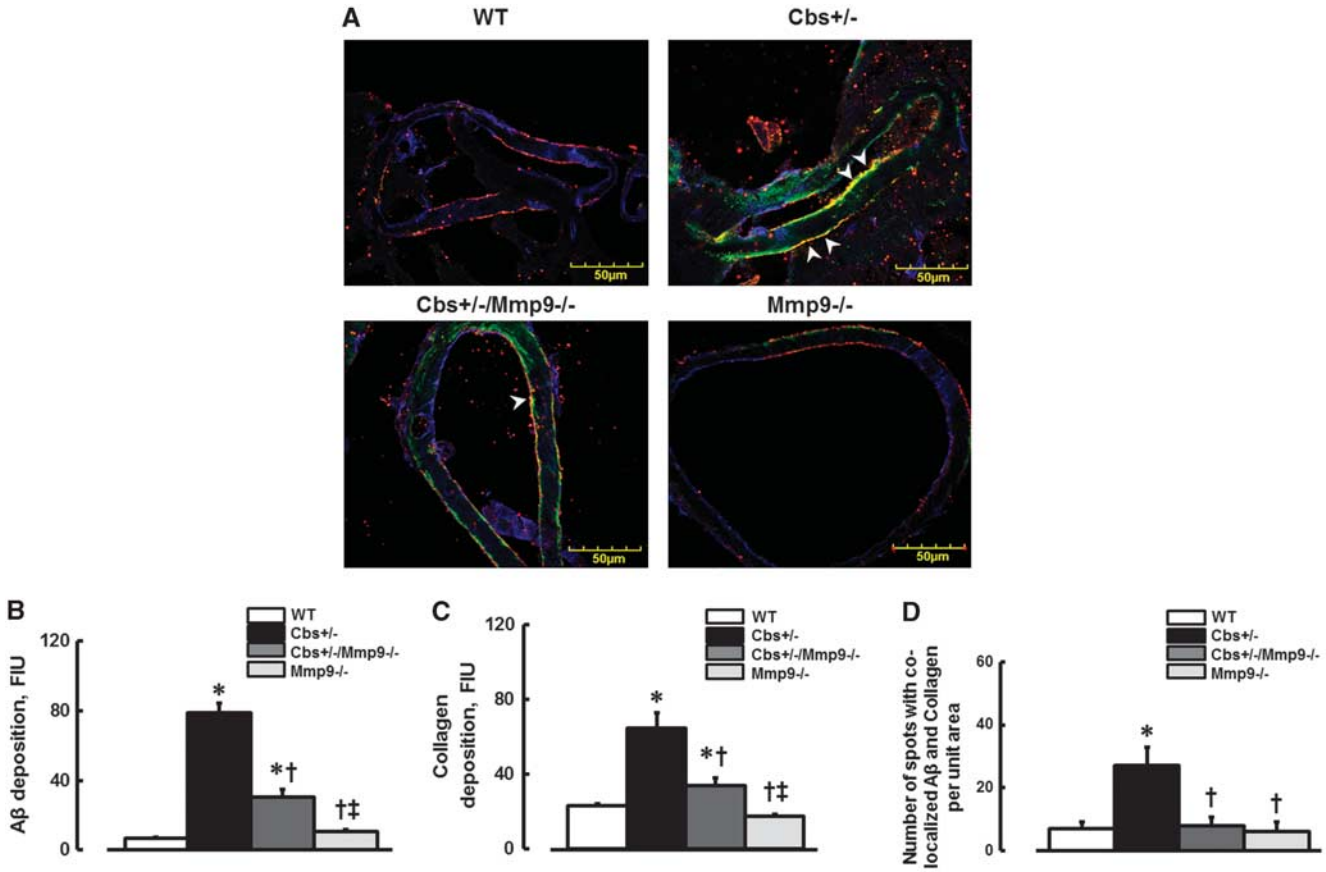

Figure 5. Deposition of amyloid beta (Aβ) on vascular collagen in mouse brain vessels. (**A**) Examples of vessel images in samples obtained from wild type (WT), Cbs$+/-$, Cbs$+/-$, and matrix metalloproteinase-9 (Mmp9$-/-$) double knockout (Cbs$+/-$/Mmp9$-/-$), and *MMP9* gene knockout (Mmp9$-/-$) mice. Deposition of Aβ (green) and collagen (red) and their co-localization (shown in yellow and indicated by arrowheads) was assessed by measuring fluorescence intensities of Aβ (green) and collagen (red) and number of spots with co-localized green and red colors after deconvolution of images. (**B**) Summary of Aβ deposition assessment. (**C**) Summary of collagen expression assessment. (**D**) Summary of Fg and Aβ co-localization assessment. *$P<0.05$ for all, versus WT; †, versus Cbs$+/-$; ‡, versus Cbs$+/-$/Mmp9$-/-$; $n=5$ for all groups.

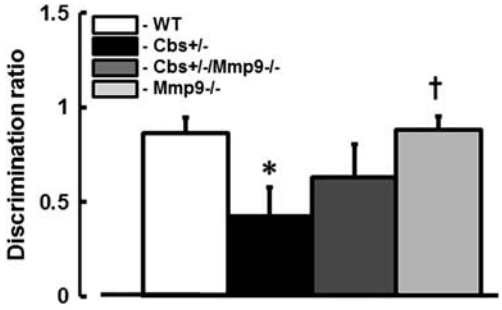

Figure 6. Hyperhomocysteinemia-induced loss of short-term memory in mice. Short-term memory of wild type (WT), Cbs$+/-$, Cbs$+/-$ and matrix metalloproteinase-9 (Mmp9$-/-$) double knockout (Cbs$+/-$/Mmp9$-/-$), and *MMP9* gene knockout (Mmp9$-/-$) mice was assessed by novel object recognition test. Lower discrimination ratio indicates impaired short-term memory. *$P<0.05$ for all, versus WT; †, versus Cbs$+/-$; $n=10$ for all groups.

Previously, we have shown that an acute injection of Hcy and the resultant elevation of its blood content caused cerebrovascular protein leakage in mice.[17,31] In the present study, cerebrovascular leakage to FITC-BSA was studied in genetic model of mouse HHcy. In both cases, HHcy resulted in enhanced cerebrovascular permeability. Others have reported effect HHcy on retinal vascular permeability.[47] Combined, these results suggest that HHcy increases vascular permeability in most of the organs. However, as Fg–Aβ complex has a greater effect on central nervous system, its effect in other organs e.g., skeletal muscle, can be less prominent.

Results of the present study indicate that HHcy, via activation of MMP9, predominantly influences expression and possibly causes translocation of JPs such as VE-cadherin into the cytosol. These results coincide with our previous findings showing that HHcy increases permeability of human intestinal microvascular EC monolayer, which was associated with downregulation of VE-cadherin.[37] Changes in cell JP expressions in addition to their possible translocations to cytosol by the formed filamentous actin[37] suggest a greater role of paracellular transport pathway during HHcy. We previously found that elevated level of Hcy decreased EC layer integrity (defined by changes in trans-endothelial electrical resistance) suggesting the wider opening of gaps between the ECs.[37] The present data confirmed results of our other study where we showed that HHcy increased overall pial venular protein leakage; however, we were unable to differentiate paracellular from transcellular transport.[17]

Finding that absence of MMP9 activity ameliorated the effect of HHcy on paracellular transport and on overall cerebrovascular

permeability, indicates that HHcy-induced activity of MMP9 affects EC JPs enhancing the cerebrovascular permeability. In fact, HHcy-induced downregulation of EC JP VE-cadherin was lesser in the absence of MMP9 activity. The role of MMP9 activity in regulation of VE-cadherin has been shown previously.[48] We also have shown that expression of VE-cadherin in mouse pial vessels is lower in the absence of MMP9 activity.[29] Thus, our results confirm a strong involvement of MMP9 activity in regulation of EC JPs and the resultant cerebrovascular permeability to proteins via paracellular transport pathway.

It has been shown that MMP9 can compartmentalize in caveolae structure[49] suggesting that it can be involved in the formation of functional caveolae. In our previous study, we found that HHcy activated formation of functional caveolae in human intestinal ECs and this effect of Hcy was abrogated if activity of MMP9 was inhibited.[37] We found that HHcy can affect both paracellular and transcellular transports.[37] However, at that time, we were unable to identify prevailing role of one or another transport pathway in overall permeability of intestinal EC layer.[37] In the present study, we showed that HHcy results in increased cerebrovascular permeability via mainly the paracellular transport and has lesser effect on caveolae formation. It has been shown that increasing levels of Cav-1 do not necessarily increase number of caveolae in the endothelium.[10] In the present study, we did not find significant increase in Cav-1 level induced by high content of Hcy in brain samples or vessels of Cbs+/− mice suggesting that HHcy did not affect caveolae formation in the mouse brain cortical vessels. Therefore, it was unexpected that absence of MMP9 activity had no effect on expression of Cav-1 and as a result on formation of caveolae. Our previous finding that HHcy enhances formation of functional caveolae and increases junctional gaps in cultured human intestinal microvascular ECs[37] points to the difference between human intestinal ECs, which are prone to enhanced permeability, and ECs of mouse cerebral vessels that are more resistant to effects of HHcy.

Other members of the caveolin family of proteins such as Cav-2 and Cav-3 have also been found in brain tissue.[50] However, while Cav-1 and Cav-2 are most abundantly expressed in brain ECs, Cav-1 and Cav-3 were found in brain astroglial cells.[50] While expression of Cav-1 or Cav-3 is necessary for the formation of caveolae, expression of Cav-2 is not required and its role is not clear.[51] These data indicate a prevailing role of Cav-1 (over Cav-2 and Cav-3) in regulation of endothelial transcytosis and the resultant vascular permeability.

Upregulation of PV-1 in brain vasculature during BBB disruption in rodents has already been demonstrated.[52] Although we found that HHcy increases cerebrovascular permeability, it has lesser effect on PV-1. Similarly, HHcy did not have an effect on Cav-1 expression, and as a result, had a limited effect on Cav-1 and PV-1 co-localization (i.e., caveolae formation). These results along with our direct observation of brain pial vascular permeability changes suggest that increased cerebrovascular permeability during HHcy occurs via mainly the paracellular transport pathway.

The results of our immunohistochemistry analyses done on brain samples showed that HHcy increased formation of Fg–Aβ complex that could be a result of increased cerebrovascular permeability and the resultant leakage of Aβ and mainly of Fg, which is the larger protein, to SEM and/or interstitium. Increased accumulation of Fg and Aβ would lead to favorable conditions for Fg–Aβ complex formation. Formation of this complex was significantly lesser in the absence of MMP9 activity suggesting a role of MMP9 activation in the cerebrovascular permeability and subsequent possible accumulation of Fg–Aβ complexes.

It has been shown that level of Aβ in the cortex or hippocampus was not affected by high-Hcy diet.[53] These results obtained from mouse brain tissue samples are contrary to our findings of increased formation of Fg–Aβ complex in brain vasculature of Cbs+/− mice defined by immunohistochemistry. These discrepancies could be a result of high abundance of Aβ in blood.[54] In addition, there was no attempt to define formation of Fg–Aβ complex, which most likely occurs in the vicinity of a vessel. Therefore, immunohistochemical analysis of brain samples with flushed vasculature after the experiments (as in the present study), where Fg–Aβ complex can be identified in SEM or adjacent to the vessel interstitium, is the better way to define association of Fg and Aβ.

One of the manifestations of vascular remodeling is alteration of collagen content in SEM. It has been found that level of collagen is increased in cerebral microvessels during Alzheimer's disease.[28] Although the biologic function and the contribution of collagen to the pathogenesis of Alzheimer's disease and Aβ plaque formation are unknown, collagen biding to Aβ has been documented.[25] Thus, collagen can be a base matrix for Fg–Aβ complex deposition in SEM. Our data show that HHcy increased association of Aβ with vascular collagen in brain samples, and this effect was ameliorated in the absence of MMP9 activity. These results suggest that HHcy-induced increased cerebrovascular permeability leads to an enhanced deposition of Fg on SEM collagen and formation of Fg–Aβ-collagen complex.

Our findings of increased formation of Fg–Aβ complex in the vicinity of the cerebral vessels during HHcy are associated with loss of short-term memory in Cbs+/− mice. Contrary to the expected improvement, although there was a tendency, an absence of MMP9 activity did not ameliorate the loss of memory in mice with an elevated level of Hcy. These results suggest that absence of MMP9 activity during HHcy, as it affects mainly the paracellular transport and to a lesser extent a protein transcytosis, has a moderate effect on overall cerebrovascular permeability to large proteins. In addition, besides an enhanced cerebrovascular

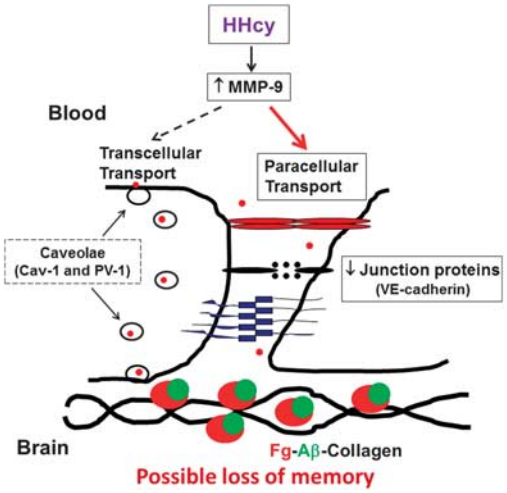

Figure 7. Possible mechanism of hyperhomocysteinemia (HHcy)-induced formation of fibrinogen–amyloid β (Fg–Aβ)-collagen complex formation. HHcy increases activity of matrix metalloproteinase-9 (MMP-9), which enhances cerebrovascular permeability mainly through paracellular transport pathway down regulating VE-cadherin. Increased vascular permeability leads to accumulation of Fg in subendothelial matrix and promotes its binding to Aβ and collagen resulting in formation of Fg–Aβ-collagen complex, which can be involved in short-term memory loss. Note: The schematic model depicting the possible mechanism of Fg–Aβ complex formation during HHcy presented above is not specific to brain vessels. However, brain is the place where Fg–Aβ complex formation and its possible association with neuronal cells have the most devastating effect.

permeability that can lead to an increased accumulation of Fg–Aβ complex in brain, HHcy causes other neurodestructive effects. Recent study showed that HHcy causes cognitive impairment without increasing in levels of Aβ in brain tissue.[55,56] However, no association of Aβ with Fg or association of Aβ and Fg with brain vessels and cerebrovascular permeability to large proteins were tested. Use of Evans blue, which is a marker of paracellular transport mainly of small molecules, did not allow assessment of vascular wall crossing such molecules as albumin or Fg. They showed that *Cbs* deficient mice had a poor spatial memory compared with the controls.[55] However distribution of Aβ in brain tissue and particularly its accumulation near the cerebral vessels was not investigated. In present study, we showed that Fg–Aβ complex formation is increased in cerebrovascular vicinity (most likely in SEM) indicating that it can alter vasculoneuronal interaction. Combined with our results, data of Rhodehouse *et al*[55,56] suggest that HHcy causes impairment of memory affecting more than one pathway such as cerebrovascular permeability and Fg–Aβ complex formation.

In conclusion, our data confirm previous findings[17,31] and show that HHcy increases cerebrovascular permeability. However, contrary to HFg, the other type of inflammatory pathology, which mainly affects caveolar transcytosis,[30] HHcy enhances protein leakage via mainly the paracellular transport pathway. In general, the paracellular transport activity is usually of a transient nature, and when activated, it demonstrates biphasic trend in alterations of JPs and the loss BBB functional integrity.[57] It has been shown that biphasic opening of the junctional gaps to blood proteins (that can last from minutes to days) can be induced by various pathologic stimulations.[57] An extent and duration of the gap openings depends on degree and duration of an inducing pathology.[57] Our data support the hypothesis that HHcy can be a strong factor leading to increased cerebrovascular gap openings (Figure 7).

Limitations of the Study

As we measured only the relative fluorescence intensity in the interstitial space adjacent to a pial venule and did not evaluate hydrostatic pressure in the venule, we could not asses the venular permeability to solutes as required by the Starling's concept. However, the presented data indicate accumulation of FITC and Alexa 647-BSA in interstitium, which can be considered an adequate measure for a venular permeability to the tracers. In addition, we present data that reflect changes in tracers' fluorescence intensities inside and outside of the vascular segment. This enhances the accuracy of the measurement.

Although it has been shown that VE-cadherin has a prevailing role in changes of vascular permeability for cells and substances,[40] alterations in paracellular transport still involve changes in all the JPs including tight, gap, and adherence JPs. We have already shown effects of HHcy on EC JPs such as occludin, ZO-1, connexin-43, and VE-cadherin.[37,39] However, further studies are needed to observe possible alterations of JPs other than VE-cadherin (e.g., claudin, zonula occludin-2, connexin-40) during HHcy-induced increased cerebrovascular permeability.

Our conclusions that increased cerebrovascular permeability to proteins can lead to Fg–Aβ complex formation are based on direct observations of pial vessels. This effect presumably occurs in whole brain circulation including the hippocampus, which is directly associated with memory. Therefore, further studies are needed to directly observe changes in microvascular permeability to large proteins in hippocampus.

DISCLOSURE/CONFLICT OF INTEREST

The authors declare no conflict of interest.

REFERENCES

1 Tyagi S. Homocyst(e)ine and heart disease: pathophysiology of extracellular matrix. *Clin Exp Hypertens* 1999; **21**: 181–198.
2 Woo KS, Chook P, Lolin YI, Cheung ASP, Chan LT, Sun YY *et al.* Hyperhomocyst(e)inemia is a risk factor for arterial endothelial dysfunction in humans. *Circulation* 1997; **96**: 2542–2544.
3 Ji C, Kaplowitz N. Hyperhomocysteinemia, endoplasmic reticulum stress, and alcoholic liver injury. *World J Gastroenterol* 2004; **10**: 1699–1708.
4 Lawrence de Koning AB, Werstuck GH, Zhou J, Austin RC. Hyperhomocysteinemia and its role in the development of atherosclerosis. *Clin Biochem* 2003; **36**: 431–441.
5 van Beynum IM, Smeitink JAM, den Heijer M, te Poele Pothoff MTWB, Blom HJ. Hyperhomocysteinemia: a risk factor for ischemic stroke in children. *Circulation* 1999; **99**: 2070–2072.
6 Mehta D, Malik AB. Signaling mechanisms regulating endothelial permeability. *Physiol Rev* 2006; **86**: 279–367.
7 Lominadze D, Dean WL, Tyagi SC, Roberts AM. Mechanisms of fibrinogen-induced microvascular dysfunction during cardiovascular disease. *Acta Physiol Scand* 2010; **198**: 1–13.
8 Simionescu M, Popov D, Sima A. Endothelial transcytosis in health and disease. *Cell Tissue Res* 2009; **335**: 27–40.
9 Stan RV. Endothelial stomatal and fenestral diaphragms in normal vessels and angiogenesis. *J Cell Mol Med* 2007; **11**: 621–643.
10 Bauer PM, Yu J, Chen Y, Hickey R, Bernatchez PN, Looft-Wilson R *et al.* Endothelial-specific expression of caveolin-1 impairs microvascular permeability and angiogenesis. *Proc Natl Acad Sci USA* 2005; **102**: 204–209.
11 Vestweber D. VE-Cadherin: the major endothelial adhesion molecule controlling cellular junctions and blood vessel formation. *Arterioscler Thromb Vasc Biol* 2008; **28**: 223–232.
12 Tuma PL, Hubbard AL. Transcytosis: crossing cellular barriers. *Physiol Rev* 2003; **83**: 871–932.
13 Parton R, Simons K. The multiple faces of caveolae. *Nat Rev Mol Cell Biol* 2007; **8**: 185–194.
14 Sverdlov M, Shajahan AN, Minshall RD. Tyrosine phosphorylation-dependence of caveolae-mediated endocytosis. *J Cell Mol Med* 2007; **11**: 1239–1250.
15 Hnasko R, McFarland M, Ben-Jonathan N. Distribution and characterization of plasmalemma vesicle protein-1 in rat endocrine glands. *J Endocrinol* 2002; **175**: 649–661.
16 Yu J, Bergaya S, Murata T, Alp IF, Bauer MP, Lin MI *et al.* Direct evidence for the role of caveolin-1 and caveolae in mechanotransduction and remodeling of blood vessels. *J Clin Invest* 2006; **116**: 1284.
17 Lominadze D, Roberts AM, Tyagi N, Tyagi SC. Homocysteine causes cerebrovascular leakage in mice. *Am J Physiol Heart Circ Physiol* 2006; **290**: H1206–H1213.
18 Rosell A, Ortega-Aznar A, Alvarez-Sabin J, Fernandez-Cadenas I, Ribo M, Molina CA *et al.* Increased brain expression of matrix metalloproteinase-9 after ischemic and hemorrhagic human stroke. *Stroke* 2006; **37**: 1399–1406.
19 Seshadri S, Beiser A, Selhub J, Jacques PF, Rosenberg IH, D'Agostino RB *et al.* Plasma homocysteine as a risk factor for dementia and Alzheimer's disease. *N Engl J Med* 2002; **346**: 476–483.
20 Vinters HV. Cerebral amyloid angiopathy. A critical review. *Stroke* 1987; **18**: 311–324.
21 Thal DR, Griffin WS, Vos RI, Ghebremedhin E. Cerebral amyloid angiopathy and its relationship to Alzheimer's disease. *Acta Neuropathol* 2008; **115**: 599–609.
22 Greenberg SM, Gurol ME, Rosand J, Smith EE. Amyloid angiopathy-related vascular cognitive impairment. *Stroke* 2004; **35**(11 suppl 1): 2616–2619.
23 Eketjäll S, Janson J, Jeppsson F, Svanhagen A, Kolmodin K, Gustavsson S *et al.* AZ-4217: a high potency BACE inhibitor displaying acute central efficacy in different *in vivo* models and reduced amyloid deposition in Tg2576 mice. *J Neurosci* 2013; **33**: 10075–10084.
24 Jiang Y, Brody D. Administration of COG1410 reduces axonal amyloid precursor protein immunoreactivity and microglial activation after controlled cortical impact in mice. *J Neurotrauma* 2012; **29**: 2332–2341.
25 van Oijen M, Witteman JC, Hofman A, Koudstaal PJ, Breteler MMB. Fibrinogen is associated with an increased risk of Alzheimer disease and vascular dementia. *Stroke* 2005; **36**: 2637–2641.
26 Ahn HJ, Zamolodchikov D, Cortes-Canteli M, Norris EH, Glickman JF, Strickland S. Alzheimer's disease peptide β-amyloid interacts with fibrinogen and induces its oligomerization. *Proc Natl Acad Sci USA* 2010; **107**: 21812–21817.
27 Sen U, Mishra P, Tyagi N, Tyagi S. Homocysteine to hydrogen sulfide or hypertension. *Cell Biochem Biophys* 2010; **57**: 49–58.
28 Kalaria RN, Pax AB. Increased collagen content of cerebral microvessels in Alzheimer's disease. *Brain Res* 1995; **705**: 349–352.
29 Muradashvili N, Qipshidze N, Munjal C, Givvimani S, Benton RL, Roberts AM *et al.* Fibrinogen-induced increased pial venular permeability in mice. *J Cereb Blood Flow Metab* 2012; **32**: 150–163.

30 Muradashvili N, Tyagi R, Lominadze D. A dual-tracer method for differentiating transendothelial transport from paracellular leakage *in vivo* and *in vitro*. *Front Physiol* 2012; **3**: 166–172.
31 Lominadze D, Tyagi N, Sen U, Ovechkin A, Tyagi S. Homocysteine alters cerebral microvascular integrity and causes remodeling by antagonizing GABA-A receptor. *Mol Cell Biochem* 2012; **371**: 89–96.
32 Muradashvili N, Benton R, Tyagi S, Lominadz D. Elevated level of fibrinogen increases caveolae formation; Role of matrix metalloproteinase-9. *Cell Biochem Biophys* 2013; **69**: 283–294.
33 Bevins RA, Besheer J. Object recognition in rats and mice: a one-trial non-matching-to-sample learning task to study 'recognition memory'. *Nat Protoc* 2006; **1**: 1306–1311.
34 Kundu S, Kumar M, Sen U, Mishra PK, Tyagi N, Metreveli N *et al.* Nitrotyrosinylation, remodeling and endothelial-myocyte uncoupling in iNOS, cystathionine beta synthase (CBS) knockouts and iNOS/CBS double knockout mice. *J Cell Biochem* 2009; **106**: 119–126.
35 Yoo J-H, Lee S-C. Elevated levels of plasma homocyst(e)ine and asymmetric dimethylarginine in elderly patients with stroke. *Atherosclerosis* 2001; **158**: 425–430.
36 Sauls DL, Lockhart E, Warren ME, Lenkowski A, Wilhelm SE, Hoffman M. Modification of fibrinogen by homocysteine thiolactone increases resistance to fibrinolysis: a potential mechanism of the thrombotic tendency in hyperhomocysteinemia. *Biochemistry*. 2006; **45**: 2480–2487.
37 Munjal C, Tyagi N, Lominadze D, Tyagi S. Matrix metalloproteinase-9 in homocysteine-induced intestinal microvascular endothelial paracellular and transcellular permeability. *J Cell Biochem* 2012; **113**: 1159–1169.
38 Markoutsa E, Papadia K, Clemente C, Flores O, Antimisiaris SG. Anti-Aβ-MAb and dually decorated nanoliposomes: effect of Aβ1-42 peptides on interaction with hCMEC/D3 cells. *Eur J Biopharm* 2012; **81**: 49–56.
39 Kamat PK, Kalani A, Givvimani S, Sathnur PB, Tyagi SC, Tyagi N. Hydrogen sulfide attenuates neurodegeneration and neurovascular dysfunction induced by intracerebral-administered homocysteine in mice. *Neuroscience* 2013; **252**: 302–319.
40 Dejana E, Orsenigo F, Lampugnani MG. The role of adherens junctions and VE-cadherin in the control of vascular permeability. *J Cell Sci* 2008; **121**: 2115–2122.
41 Munjal C, Givvimani S, Qipshidze N, Tyagi N, Falcone JC, Tyagi SC. Mesenteric vascular remodeling in hyperhomocysteinemia. *Mol Cell Biochem* 2011; **348**: 99–108.
42 Sen U, Tyagi N, Kumar M, Moshal KS, Rodriguez WE, Tyagi SC. Cystathionine-β-synthase gene transfer and 3-deazaadenosine ameliorate inflammatory response in endothelial cells. *Am J Physiol Cell Physiol* 2007; **293**: C1779–C1787.
43 Bell RD, Winkler EA, Singh I, Sagare AP, Deane R, Wu Z *et al.* Apolipoprotein E controls cerebrovascular integrity via cyclophilin A. *Nature* 2012; **485**: 512–516.
44 Bell RD, Winkler EA, Sagare AP, Singh I, LaRue B, Deane R *et al.* Pericytes control key neurovascular functions and neuronal phenotype in the adult brain and during brain aging. *Neuron* 2010; **68**: 409–427.
45 Jakubowski H. Pathophysiological consequences of homocysteine excess. *J Nutr* 2006; **136**(6 Suppl): 1741S–1749S.
46 Ho PI, Collins SC, Dhitavat S, Ortiz D, Ashline D, Rogers E *et al.* Homocysteine potentiates β-amyloid neurotoxicity: role of oxidative stress. *J Neurochem* 2001; **78**: 249–253.
47 Tawfik A, Al-Shabrawey M, Roon P, Sonne S, Covar JA, Matragoon S *et al.* Alterations of retinal vasculature in cystathionine-Beta-synthase mutant mice, a model of hyperhomocysteinemia. *Invest Ophthalmol Vis Sci* 2013; **54**: 939–949.
48 Navaratna D, McGuire PG, Menicucci G, Das A. Proteolytic degradation of VE-cadherin alters the blood-retinal barrier in diabetes. *Diabetes* 2007; **56**: 2380–2387.
49 Phillips PG, Birnby LM. Nitric oxide modulates caveolin-1 and matrix metalloproteinase-9 expression and distribution at the endothelial cell/tumor cell interface. *Am J Physiol Lung Cell Mol Physiol* 2004; **286**: L1055–L1065.
50 Ikezu T, Ueda H, Trapp BD, Nishiyama K, Sha JF, Volonte D *et al.* Affinity-purification and characterization of caveolins from the brain: Differential expression of caveolin-1, -2, and -3 in brain endothelial and astroglial cell types. *Brain Res* 1998; **804**: 177–192.
51 Sowa G, Xie L, Xu L, Sessa W. Serine 23 and 36 phosphorylation of caveolin-2 is differentially regulated by targeting to lipid raft/caveolae and in mitotic endothelial cells. *Biochemistry* 2008; **47**: 101–111.
52 Shue E, Carson-Walter E, Liu Y, Winans B, Ali Z, Chen J *et al.* Plasmalemmal vesicle associated protein-1 (PV-1) is a marker of blood-brain barrier disruption in rodent models. *BMC Neurosci* 2008; **9**: 29.
53 Bernardo A, McCord M, Troen AM, Allison JD, McDonald MP. Impaired spatial memory in APP-overexpressing mice on a homocysteinemia-inducing diet. *Neurobiol Aging* 2007; **28**: 1195–1205.
54 Kiko T, Nakagawa K, Satoh A, Tsuduki T, Furukawa K, Arai H *et al.* Amyloid β levels in human red blood cells. *PLoS One* 2012; **7**: e49620.
55 Rhodehouse BC, Erickson MA, Banks WA, Bearden SE. Hyperhomocysteinemic mice show cognitive impairment without features of Alzheimer's Disease phenotype. *J Alzheimers Dis* 2013; **35**: 59–66.
56 Rhodehouse BC, Mayo JN, Beard Jr RS, Chen C-H, Bearden SE. Opening of the blood-brain barrier before cerebral pathology in mild hyperhomocysteinemia. *PLoS One* 2013; **8**: 1–7.
57 Sandoval KE, Witt KA. Blood-brain barrier tight junction permeability and ischemic stroke. *Neurobiol Dis* 2008; **32**: 200–219.